# FIRST DEMONSTRATION OF NOVEL TECHNIQUE FOR DISRUPTION MITIGATION BY CORE IMPURITY DEPOSITION USING SHELL PELLETS ON DIII-D

N.W. Eidietis, N. Alexander, P.B. Parks
General Atomics
San Diego, USA
Email: eidietis@fusion.gat.com

E.M. Hollmann, R.A. Moyer
University of California San Diego
San Diego, USA

J.L. Herfindal, D. Shiraki
Oak Ridge National Laboratory
Oak Ridge, USA

A. Lvovksiy
Oak Ridge Associated Universities
Oak Ridge, USA

V.A. Izzo
Fiat Lux
San Diego, USA

**Abstract**

Disruption mitigation by core impurity deposition using novel shell pellet technology has been demonstrated for the first time on DIII-D. This provides a new method of "inside-out" radiative cooling of the plasma, which NIMROD non-linear MHD simulations predict to (i) provide high impurity assimilation and radiated energy fraction to protect the divertor from conducted thermal loads, (ii) allow the use of low-Z impurities to moderate the current quench rate and associated forces, and (iii) create globally stochastic field lines at high densities to suppress runaway electron seed formation. This transforms the physics mechanisms and the prospects for safe mitigation of disrupting plasmas for ITER and the tokamak generally. The shell pellet technique utilizes a thin, minimally-perturbative shell to transport the enclosed radiating impurity (boron dust) to the plasma core before dispersal, delaying the onset of global MHD that is typically initiated by conventional edge-cooling techniques (e.g. massive gas or shattered pellet injection), where most of the particles do not reach the core. Imaging provides clear evidence of the boron dust impurity payload being deposited deep within the plasma core, with inverted $T_e$ profile data providing evidence for an "inside-out" mitigation process. Pellet deposition depth is consistent with existing 1D modeling. Mitigation metrics are shown to improve with increased pellet velocity and deposition depth, with decreased heat loads to the divertor, and reduced current perturbations in the quench, and increased impurity particle assimilation fractions approaching unity, indicating the importance of core impurity deposition. Future work and the design of ITER-relevant shells are discussed. These initial experiments provide a first proof-of-principle that this new mitigation technology may address major shortcomings in the edge-cooling shattered pellet injection presently planned for ITER and provide an effective solution for future fusion reactors.

## 1. INTRODUCTION

Disruption mitigation remains a critical challenge for ITER [1] and any future burning plasma tokamak. Successful mitigation requires a delicate balance, in that it must isotropically radiate the plasma thermal energy before it is conducted to the divertor in the thermal quench (TQ), produce a moderately warm current quench (CQ) so that the resulting eddy currents do not cause gross structural damage, and at the same time provide sufficient density to suppress runaway electron (RE) generation and growth.

Conventional "outside-in" disruption mitigation techniques such as massive gas injection (MGI) [2-5] or shattered pellet injection (SPI, the ITER baseline mitigation technology) [6, 7] deposit radiating impurities near the plasma edge and rely upon global MHD induced when the resulting cooling front passes the q=2 surface to mix the radiating impurities into the core and radiate the plasma thermal energy ($W_{th}$) [8, 9]. This process presents an undesirable condition wherein the very MHD activity that requires mitigation is also critical for impurity transport to the core. The MHD mixing process typically results in fairly low impurity assimilation (<20%), requiring high-

Z (neon or higher Z) impurities to adequately radiate $W_{th}$, and limiting the total density available for runaway electron (RE) suppression [10, 11].

Core impurity deposition, wherein the primary radiating impurity is transported to the plasma core without significant edge cooling or MHD mixing (Fig. 1), shows promise to address the above shortcomings of conventional "outside-in" mitigation techniques. NIMROD non-linear 3D resistive MHD modeling [12] predicts core radiation will invert the thermal quench process, cooling from the inside-out and minimizing heat transport to the scrape-off layer to protect the divertor. Reaching 100% impurity assimilation enables the use of low-Z impurities to achieve high thermal radiation fraction while still providing acceptably slow current decay to avoid mechanical damage from eddy currents. In addition, NIMROD predicts achieving global stochasticity throughout the entire plasma cross-section (Fig. 2), which coupled with high core densities will suppresses RE formation.

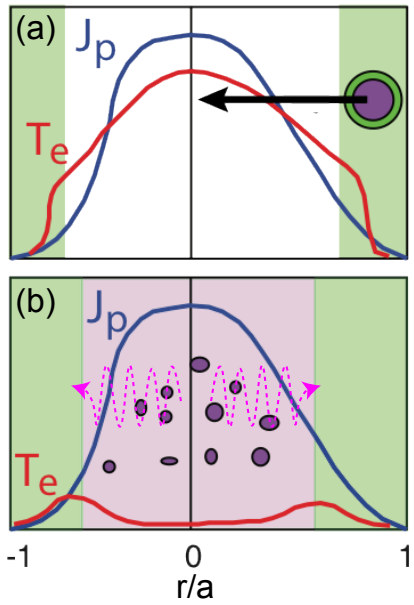


FIG. 1 Conceptual sketch of shell pellet method. (a) Radiating impurity dust (purple circle) is encased in low-Z shell (green) in order to transport impurities through peaked plasma $T_e$ profile without volumetric impurity radiation until (b) the shell ablates.

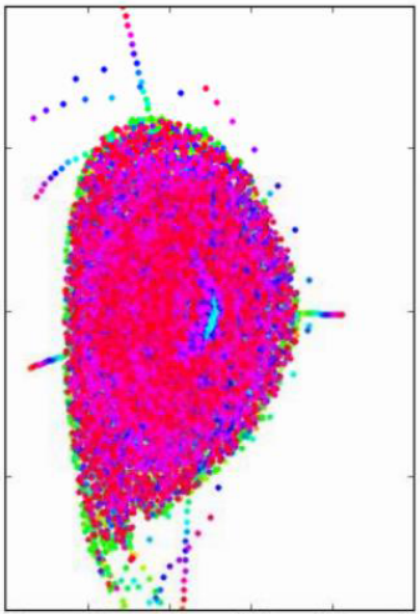

FIG. 2 NIMROD DIII-D simulation. Poincare plot of field lines 0.1ms after Ar impurity deposited near but off-center from core.

This work presents the first demonstration of core impurity deposition using shell pellet injection techology for disruption mitigation on DIII-D. These initial experiments provide an early proof-of-principle that this new mitigation technology may address the major shortcomings described above of the conventional edge-cooling shattered pellet injection presently planned for ITER and provide an effective solution for future fusion reactors.

## 2. EXPERIMENTAL SETUP

The experiments described below utilize 40μm thick, 3.7mm outer diameter diamond shells filled with a 20mg boron powder payload (Fig. 3) pneumatically launched at velocities up to 250 m/s. A 500μm diameter hole is drilled into each shell to allow the boron powder fill, and then sealed with a polymer glue. Sifting of the boron powder guaranteed a grain diameter less than 44μm, resulting in a packing fraction of 30-35% that determined the maximum boron fill mass. These diamond shells were developed to provide greater mechanical strength and

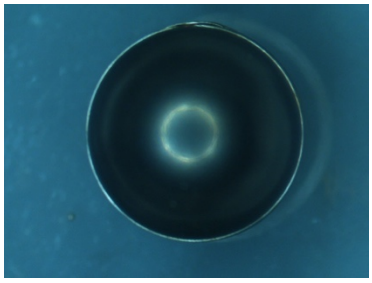

FIG. 3 Visible image of 3.7mm outer diameter, 40μm thick, boron-filled diamond shell. Glue cap is uneven patch at top of shell.

higher ionization potential than the polystyrene shells used in previous attempts at shell pellet mitigation [13], which proved too weak to survive injection forces unless they were manufactured with walls too thick to fully ablate within the plasma.

The target plasma for this work is a lower single null super H-mode [14] configuration with plasma current $I_p$ = 1.5MA. The shell pellet is injected during the transition from L-mode to super H-mode at thermal energy $W_{th}$ ~ 0.9MJ. The super H-mode target is utilized in order to provide access to a wide range of $W_{th}$, although the present study only reports on the mid-energy level. Pellet penetration is measured using a tangential visible camera [15] at a frame rate of 18kHz. Thermal loads were measured using an infra-red periscope [16] and the fitting methods described in [17]. The pellet was launched from the low-field-side port approximately 9cm above the mid-plane.

## 3. DEMONSTRATION OF CORE IMPURITY DEPOSITION

The first demonstration of a shell pellet depositing its boron dust payload in the plasma core is shown in Fig. 4. Injected at a velocity of 230 m/s, the pellet reaches the plasma edge (Fig. 4, time point #1) and continues to transit the plasma as a solid shell (Fig 4, time point #2) until finally ablating and releasing its boron dust payload near the magnetic axis, well within the q=3/2 surface (Fig. 4, time point #3).

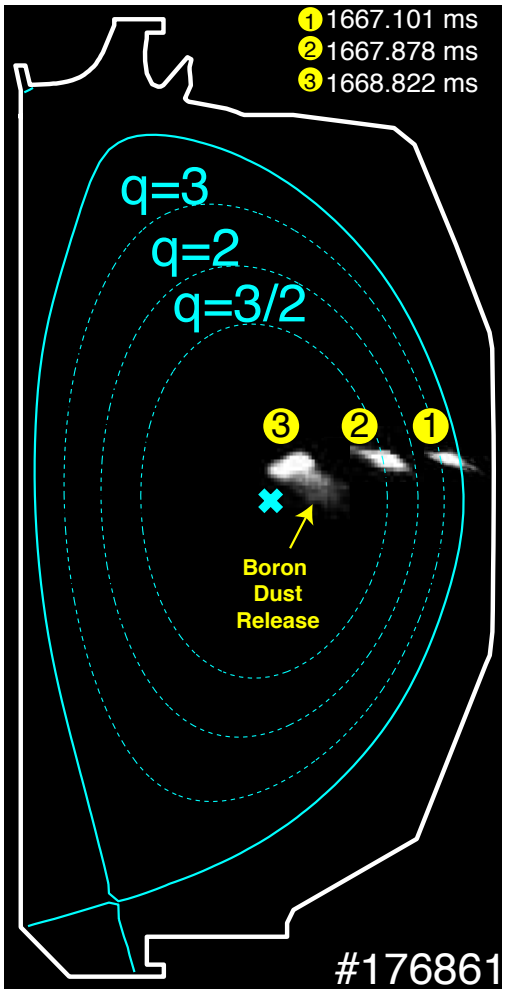


FIG. 4 Overlay of EFIT equilibrium just prior to shell injection and camera images showing shell progression from edge to core at three time points (marked with yellow circles). Boron dust release near core is noted by annotation. Shell pellet image overlays have been enlarged for detail.

Thomson scattering provides evidence for the inverted $T_e$ profile expected from "inside-out" core impurity deposition (Fig. 5). Prior to shell pellet injection, $T_e$ exhibits a typical H-mode pedestal and peaked profile (Fig. 5, red). After the pellet enters the plasma, an inverted $T_e$ profile (Fig. 5, blue) with edge $T_e > 0.25$ keV and interior $T_e < 0.1$ keV appears. This profile is expected if dominant core radiation causes thermal transport away from the edge and toward the core. It should be noted that the post-injection Thomson scattering profile was obtained before clear imaging evidence of boron dust dispersal (Fig 4, time point #3), but after the pellet crosses the q=3/2 surface.

There is uncertainty in the time of initial dust release, as light pollution from the carbon shell, finite image spatial resolution, and rotation of the shell render positive identification of the dust difficult until the dust disperses far enough to appear distinct from the shell. Hence, it is ambiguous as to whether the observed $T_e$ profile inversion is caused by the diamond shell itself or boron dust release prior to the first clear imaging evidence.

Ideally, the shell pellets should not radiate any of the plasma thermal energy prior to ablating in the core. As

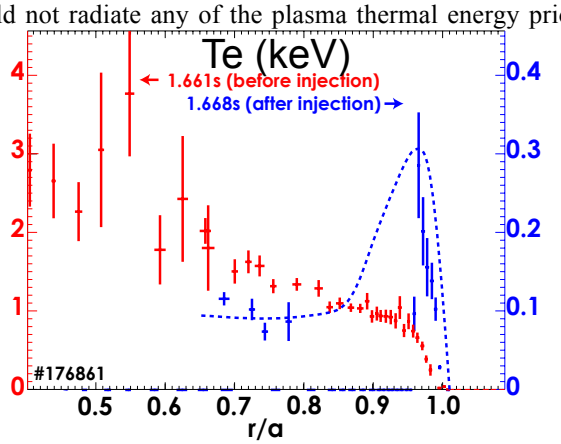


FIG. 5 Thomson scattering $T_e$ profile before (red) and after (blue) shell pellet injection. Sparsity of profile points in later profile is due to a limited number of narrow-band polychromators required for low-$T_e$, high impurity content measurements.

shown in Fig. 6, the diamond pellets utilized in this initial experiment diverge somewhat from ideal behaviour. The diamond shell begins to ablate (Fig. 6b) and radiate strongly near the injector location (Fig. 6c) shortly after passing through the plasma boundary. The neutron production rate (Fig. 6d) begins to drop gradually after the pellet passes the q=2 surface, but prior to observed dust dispersal (Fig. 6, vertical pink line). This reduction in neutron rate may be due to radiation cooling of the plasma (reduction in total thermal energy), or the result of dilution cooling (no net change in plasma thermal energy) due to the increase in density from shell ablation. Unfortunately, the strong radiated power asymmetry renders the two-point radiated power measurement insufficient for accurate energy accounting. The subsequent collapse in core $T_e$ (as shown by a core SXR channel, Fig 6e) begins just prior to the first observation of dust dispersal, making it unclear whether this final core $T_e$ collapse was initiated by the shell or the payload release. However, it should be noted that the core $T_e$ collapse

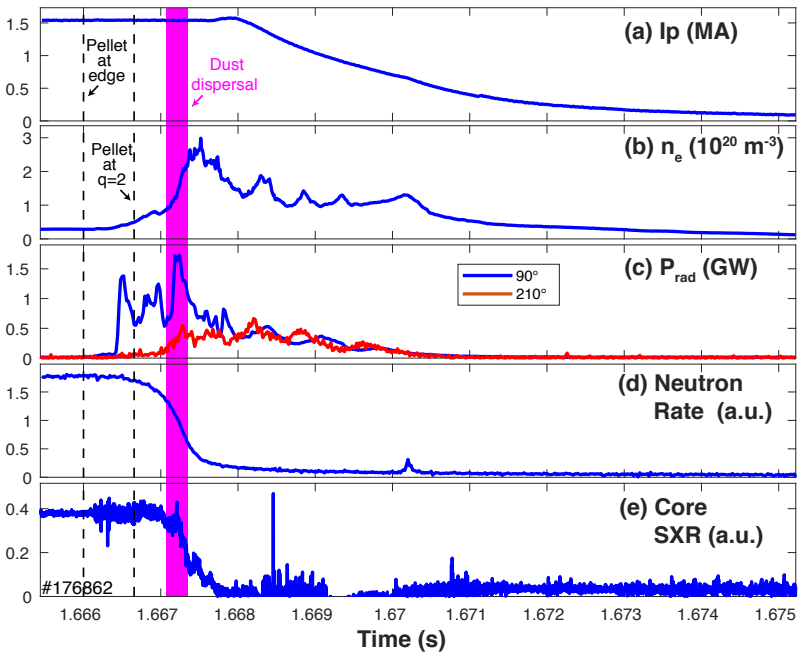


FIG. 6 Evolution of shell pellet injection discharge showing: (a) plasma current; (b) line averaged electron density; (c) radiated power at two toroidal locations; (d) neutron production rate; and (e) core SXR emission. Vertical dashed lines indicate the times of the pellet reaching the plasma edge and crossing the q=2 surface. Vertical pink region indicates the uncertainty in time at which first boron dust release is evident on imaging, with the right-most edge representing unambiguous dust release, and earlier times representing image frames where release is ambiguous.

does not begin until more than 300μs after the pellet passes through the q=2 surface, indicating deep pellet penetration before TQ MHD dominates thermal transport.

## 4. PELLET PENETRATION

The depth to which the diamond shell pellets penetrate before fully ablating is well described by modeling, within experimental variation. Pellet penetration depth is predicted for the experimental target plasma and pellet trajectory using a 1D cooling model that includes both radiation and dilution cooling on the flux surfaces, but ignores cross-field heat and particle transport. Shell ablation is calculated using pellet ablation models from [18] and [19]. As shown in Fig. 7, the normalized radius of complete shell ablation (as observed from visible camera images) agrees well with the modeling, within experimental uncertainty.

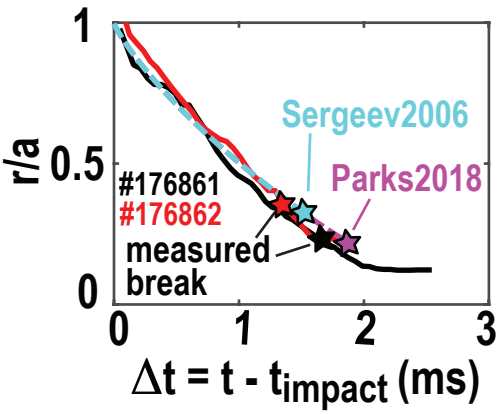


FIG. 7 Comparison of pellet penetration for two identical shell pellet shots (red and black stars) to 1D modeling of those plasma and pellet parameters, using two pellet ablation model (cyan and purple stars). Solid red and black lines indicate experimentally observed trajectories. Dashed cyan line is modeled trajectory.

As expected, increasing pellet velocity results in deeper penetration before the shell completely ablates (Fig. 8), as determined from analysis of the fast-visible camera images. The maximum attainable pellet velocity is determined by the strength of the shell structure, as increasing propellant pressure increases the accelerating force on the shell, which will eventually cause the shell to crack and disintegrate inside the injector guide tube.

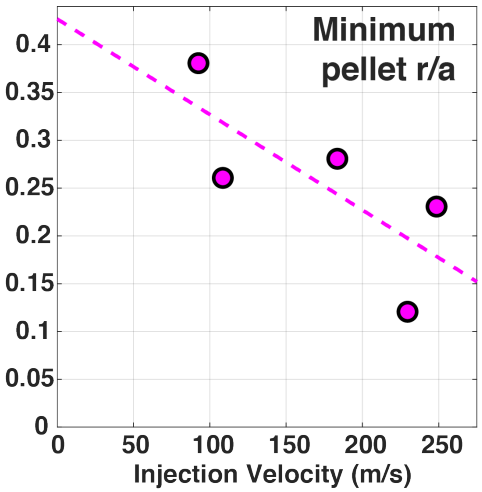


FIG. 8 Minimum minor radius of shell pellet deposition vs injection velocity.

## 5. IMPROVEMENT IN MITIGATION EFFICACY WITH INCREASING DEPTH OF DEPOSITION

The end goal of thermal quench mitigation is to reduce the heat fluence conducted to the divertor region during a disruption. Figure 9 illustrates the reduction in divertor heat fluence with increasing shell pellet injection velocity and deposition depth, as measured by the IR periscope. Two regions, one on the outer shelf and another at the inner strike point, are utilized for thermal analysis (Fig 9a). Both the shelf (Fig. 9b) and inner strike point (Fig. 9c) regions show a clear reduction in heat fluence at higher pellet injection velocity. This reduction in heat fluence indicates more effective radiation of the plasma thermal energy and reduced conduction to the divertor as the pellet deposition depth increases.

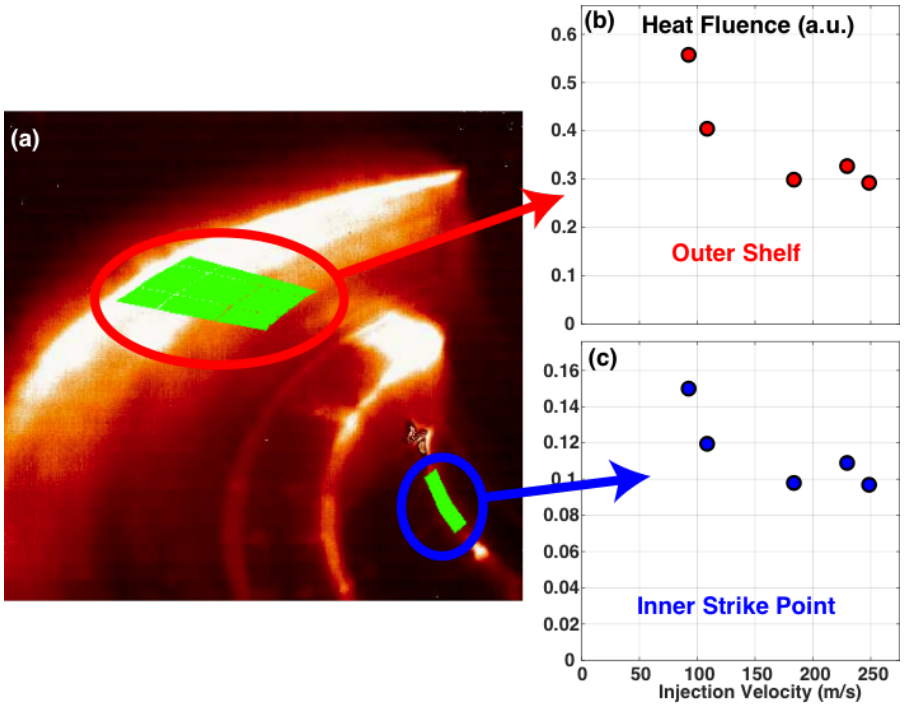


FIG. 9 (a) IR periscope image of the DIII-D lower divertor region. Green regions on the outer shelf (red circle) and inner strike point (blue circle) indicate the area over which the heat fluence measurements are averaged. (b) Heat fluence on the outer shelf region vs shell pellet injection velocity. (c) Heat fluence on the inner strike point region.

The current quench characteristics also vary with pellet injection velocity. As shown in Fig. 10a, the area-normalized current quench duration decreases with injection velocity. Reduction in the current quench duration indicates increasing resistivity in the post-TQ plasma as the pellet deposition depth increases. This is consistent with the data from Fig. 9 above, in that it indicates more effective radiation of the plasma thermal energy and a lower CQ temperature. Note the normalized CQ duration remains above the ITER allowable minimum [20], which is the point at which toroidal eddy currents are expected to cause damage to the ITER wall. In addition, the magnitude of the current spike resulting from current redistribution during the TQ decreases dramatically with increasing pellet velocity (Fig. 10b). This indicates a modification in the TQ MHD characteristics (i.e. width of current flattening region) [21, 22] as the pellet deposition depth increases.

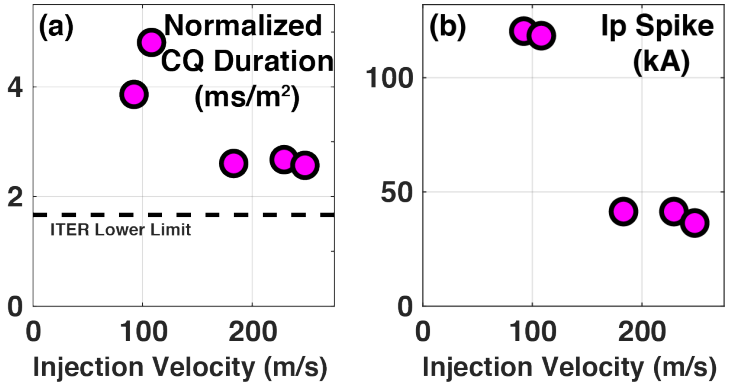


FIG. 10 (a) Current quench duration and (b) Ip spike magnitude vs injection velocity.

As noted in the introduction, a high impurity assimilation fraction is critical both to allow for the effective use of low-Z radiators and to provide high density for RE suppression. As shown in Fig. 11a, the maximum line-integrated density perturbation from the shell pellet prior to the start of the CQ increases linearly with pellet injection velocity. This may indicate either increased retention of the shell pellet atoms in the plasma or else increased ionization of those atoms as the deposition depth increases. The fraction of the total electron population provided by the diamond shell and boron payload appearing in the density perturbation is very high, increasing from 0.5 to 0.7 over the experimental range of injection velocities (Fig. 11b). As the density peak typically occurs during the TQ thermal collapse (e.g. Fig 6b and (e)), it is reasonable to assume that the impurity carbon and boron ions are not fully stripped, which implies an atomic assimilation fraction near unity for these shell pellets. Attempts to increase the injected boron mass from the ~20mg reported here to more than 300mg using larger 10mm diameter shell pellets failed due to shell failure in the guide tube. Hence, it is not yet determined if the near unity impurity assimilation fraction will remain constant as the total injected mass increases.

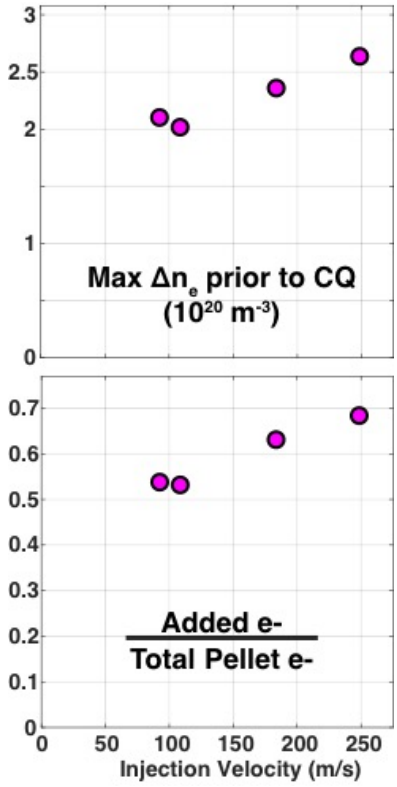


FIG. 11 (a) Maximum line-integrated density perturbation prior to start of CQ (b) Fraction of total electrons provided by diamond shell + boron dust payload observed in density perturbation, assuming an axisymmetric density distribution.

## 6. DISCUSSION AND CONCLUSIONS

Disruption mitigation by core impurity deposition using novel shell pellet technology has been demonstrated for the first time on DIII-D. These initial experiments provide empirical tests of modeling predicting improved mitigation compared to conventional "outside-in" mitigation technologies such as SPI. Imaging provides clear evidence of the boron dust impurity payload being deposited deep within the plasma core, with inverted $T_e$ profile data providing evidence for an "inside-out" mitigation process. Pellet deposition depth is consistent with existing 1D modeling. Mitigation metrics are shown to improve with increased pellet velocity and deposition depth, with increased radiation, decreased heat load to the divertor, and reduced current perturbations in the quench observed.

These results validate the basic concepts established in earlier non-linear MHD simulation projections [12] and provide a strong motivation for further exploration and development of the shell pellet disruption mitigation method. As noted in Section 5, ascertaining the scaling of the shell impurity assimilation with total mass is critical to understanding the scalability of the method. Further work is also needed to reduce the shell perturbation to the plasma, possibly through alternative shell materials or coatings, in order to better approximate "ideal" core

impurity deposition (Section 4). The enormous flexibility in the impurity composition (dust grain size and elemental composition) and its affect upon the mitigation process remains to be explored, as do the dynamics of core dust transport. Finally, development of reactor-relevant, magnetically shielded shell pellets is underway to provide deep core impurity deposition in the much more massive and energetic plasmas of ITER and future burning plasma devices [23].

Disruption mitigation using shell pellets for core impurity deposition shows early promise as an alternative for the ITER disruption mitigation system, addressing numerous shortcomings of conventional "outside-in" mitigation technologies. Continuing research is underway to refine and assess the scalability of the technology to ITER scale and compare it directly to the ITER baseline DMS technology, SPI. Nevertheless, these early results from DIII-D indicate a potentially transformative technology for the tokamak, resolving the disruption problem with high levels of core thermal radiation, tolerable forces from less perturbative current quenches, and runaway electron suppression.

## ACKNOWLEDGEMENTS

This material is based upon work supported by the U.S. Department of Energy, Office of Science, Office of Fusion Energy Sciences, using the DIII-D National Fusion Facility, a DOE Office of Science user facility, under Awards DE-FC02-04ER54698, DE-FG02-07ER54917, DE-AC05-00OR22725 and DE-AC52-07NA27344. Data shown in this paper can be obtained in digital format by following the links at https://fusion.gat.com/global/D3D_DMP.



## REFERENCES

[1] Lehnen, M., et al, J. Nucl. Mater. **463** (2015) 39–48.
[2] Hollmann E.M., et al, Nucl. Fusion **48** (2008) 115007
[3] Granetz R., et al, Nucl. Fusion **46** (2006) 1001–1008
[4] Thornton A.J., et al, Nucl. Fusion **52** (2012) 063018
[5] Pautasso G., et al, Nucl. Fusion **55** (2015) 033015
[6] Commaux N., et al, Nucl. Fusion **56** (2016) 046007
[7] Shiraki D., et al, Phys. Plasmas **23**, (2016) 062516
[8] Izzo V.A., Nucl. Fusion **46** (2006) 541–547
[9] Izzo V.A., Phys. Plasmas **20** (2013) 056107
[10] Rosenbluth M.N., Putvinski S.V., Nucl. Fusion **37** (1997) 1355-1362
[11] Martín-Solís J.R., et al, Nucl. Fusion **57** (2017) 066025
[12] Izzo V.A., Parks P.B., Phys. Plasmas **24** (2017) 060705
[13] Commaux N., et al, Nucl. Fusion **51** (2011) 103001
[14] Solomon W.M., et al, Phys. Plasmas **23** (2016) 056105
[15] Yu J.H., Van Zeeland M.A., Rev. Sci. Instrum. **79** (2008) 10F516
[16] Lasnier C.J., et al, Rev. Sci. Instrum. **85** (2014) 11D855
[17] Hollmann E.M., et al, Phys. Plasmas **22** (2015) 102506
[18] Parks P.B., "The ablation rate of some low-Z pellets with a kinetic model for the degradation of the incident plasma electrons in the surrounding ablation cloud", to be submitted to Phys. Plasmas
[19] Sergeev V.Y, et al, Plasma Phys. Rep. **32** (2006) 363-377
[20] Eidietis N.W., et al, Nucl. Fusion **55** (2015) 063030
[21] Boozer A.H., Nucl. Fusion **58** (2018) 036006
[22] Lukash V., et al, Plasma Phys. Control. Fusion **47** (2005) 2077–2086
[23] Parks P.B., "Methods and Apparatus for disruption mitigation in fusion devices", U.S. patent submitted (2018)